Published in final edited form as:
Angew Chem Int Ed Engl. 2013 October 4; 52(41): 10762–10765. doi:10.1002/anie.201305286.

β_2-adrenergic receptor activation by agonists studied with ^{19}F-NMR

Reto Horst[a,§], **Jeffrey J. Liu**[a], **Raymond C. Stevens**[a], and **Kurt Wüthrich**[a,b,*]

[a]Department of Integrative Structural and Computational Biology, The Scripps Research Institute, 10550 North Torrey Pines Road, La Jolla, CA 92037, USA

[b]Skaggs Institute for Chemical Biology, The Scripps Research Institute, 10550 North Torrey Pines Road, La Jolla, CA 92037, USA

G-protein-coupled receptors (GPCRs) recognize a wide array of orthosteric ligands in their binding site on the periplasmic cell membrane surface, initiating signal transmission through the cellular membrane to cytoplasmic partner proteins. Crystal structures of several human GPCRs in complexes with antagonists and agonists provide insights into activation-related structural rearrangements,[1] and fluorescence spectroscopy experiments indicated activation-related conformational changes in detergent-solubilized receptors.[2] ^{19}F-NMR spectroscopy and site-specific mutagenesis, as applied previously with mammalian rhodopsin,[3] more recently revealed an equilibrium between an activated state A and an inactive state I in the β_2-adrenergic receptor (β_2AR).[4] This communication now presents thermodynamic and kinetic data for this conformational equilibrium in β_2AR.

In our earlier experiments,[4] the β_2AR complexes were reconstituted in mixed micelles of *n*-dodecyl-β-*D*-maltoside (DDM) and cholesteryl hemisuccinate (CHS), with DDM:CHS = 5:1, and ^{19}F-labels were introduced by conjugation of 2,2,2-trifluoroethanethiol (TET) with cysteines near the cytoplasmic ends of the helices VI (Cys265) and VII (Cys327), and at the C-terminus (Cys341). Ligand binding assays showed that the labeled proteins retained the biological activity.[4] Sequence-specific ^{19}F-NMR assignments were based on comparison of β_2AR variants with single-residue TET-labeling, and the signal I was assigned from its high intensity in the apo-form of β_2AR and its complexes with inverse agonists.[4] Observation of the TET labels in β_2AR-complexes with different pharmacological ligands then enabled to distinguish between the activation of two different signaling pathways.[4]

A first extension of the previous work was to analyze the temperature dependence of the 1D ^{19}F-NMR spectra of β_2AR (^{TET}C265, C327S, C341A) and β_2AR (C265A, ^{TET}C327, C341A) in terms of the thermodynamic parameters that characterize the conformational equilibrium between the states A and I. This analysis was focused on complexes with agonists, i.e., norepinephrine and formoterol, since for the complexes with antagonists or inverse agonists the amplitude of the signal A is near the noise level and its volume cannot reliably be quantified. Based on the observation that the temperature dependence over the

*Corresponding author: Tel: +1 858-784-8011, Fax: +1 858 784 8014, wuthrich@scripps.edu.
§Present address: Pfizer Worldwide Research and Development, Eastern Point Road, Groton, CT, 06340, USA

range 280 K to 310 K of the NMR spectra recorded with the agonist complexes was reversible, the relative populations of the conformations represented by the signals A and I, p_A and p_I, were determined by fits to a double-Lorentzian function (Figure 1), yielding an apparent equilibrium constant, $K = p_I / p_A$. ln K was found to depend linearly on the inverse of the temperature, T (Figure 2), which is in agreement with the van't Hoff relationship between K, the molar enthalpy difference, ΔH_0, and the molar entropy difference, ΔS_0.[5]

$$\ln K = -(\Delta H_0 - \mathrm{T}S_0)/R\mathrm{T}, \quad (1)$$

where R is the gas constant. ΔH_0 values near 40 kJ/mol were obtained for both labeling sites at Cys265 and Cys327, and for both agonists used (Table 1), suggesting that the structural differences between the states A and I observed in the ^{19}F-NMR spectra (Figure 1) represent more extensive conformational rearrangements than, for example, reorientation of a single amino acid side chain. For the different systems in Table 1 the Gibbs free energy, $\Delta G_0 = -\ln(K)R\mathrm{T}$, is between 0 and 3 kJ/mol, which shows that the entropy and enthalpy terms (Table 1) nearly cancel each other. This observation is in line with the widely observed entropy–enthalpy compensation in biological systems.[6]

To investigate the exchange rates between the states A and I within the framework of a 2-state model, where k_1 and k_{-1} are the forward and reverse rate constants,

$$\mathrm{A} \underset{k_{-1}}{\overset{k_1}{\rightleftarrows}} \mathrm{I}, \quad (2)$$

we used 2D ^{19}F–^{19}F exchange spectroscopy (EXSY)[7] and 1D ^{19}F saturation transfer NMR experiments.[8] The overall exchange rate constant, k_{ex}, is given by

$$k_{ex} = k_1 + k_{-1} = k_1/p_I = k_{-1}/p_A, \quad (3)$$

where p_A and p_I are the relative populations of the states A and I. The observation of two distinct signals A and I in the ^{19}F-NMR spectra of β_2AR (Figure 1) showed that the conformational exchange is slow on the ^{19}F-NMR chemical shift time scale, so that k_{ex} satisfies the inequality,

$$k_{ex} \ll \frac{\Delta\omega}{2\sqrt{p_A p_I}}, \quad (4)$$

where $\Delta\omega$ is the chemical shift between I and A in rad/sec.[9] For TET-labeled Cys265 and Cys327 the $\Delta\omega$ values are 2×10^3 rad/sec and 4×10^3 rad/sec, respectively, and $p_A = 1-p_I$ is between 0.2 and 0.9.[4] An upper limit of $k_{ex} \leq 10^3$ s^{-1} was thus previously established, and additional support for this limit was obtained from experiments with paramagnetic shift reagents.[4] Here, 2D [^{19}F,^{19}F]-EXSY experiments with a $^{\mathrm{TET}}\beta_2$AR–isoproterenol complex were performed with mixing times of 300 and 600 ms. For k_{ex} values of 10 s^{-1} or larger, 2D [^{19}F,^{19}F]-cross-peaks between the signals A and I are predicted to be of similar size as the diagonal peaks in these experiments (Figure 3c). The absence of [^{19}F,^{19}F]-cross-peaks (Figure 3) then enabled us to establish a new upper limit of $k_{ex} < 10$ s^{-1} at 280 K. ^{19}F-NMR saturation-transfer experiments with apo- β_2AR(C265A, $^{\mathrm{TET}}$C327, C341A) at 280 K further

indicated that the exchange rate is significantly slower than 10 s^{-1}. Considering the spectral overlap of the two signals (Figure 4), we applied selective off-resonance continuous wave (cw) pre-irradiation in these experiments (Figure 4), and analyzed the resulting intensity variations of the signals A and I with model simulations based on the Bloch equations for two-site exchange (Equations (5) to (10) in the Appendix).[10] The longitudinal and transverse spin relaxation times, T_1 and T_2, used in these model computations were determined with an inversion–recovery experiment (see the Experimental Section), and from the line shapes of the signals in the 1D ^{19}F-NMR spectrum (top trace in Figure 4), respectively. Comparison of the experimental data with the simulations (Figure 5) showed that the observed decay of the signal I was due to direct saturation by the off-resonance irradiation, and that there was no measureable contribution due to coherence transfer from signal A to signal I by conformational exchange (Figure 5).

In conclusion, this paper used TET ^{19}F-NMR probes attached to three cysteine residues near the cytoplasmic surface to determine thermodynamic and kinetic parameters for the equilibrium between an active state, A, and an inactive state, I, of β_2AR, which both represent an ensemble of rapidly interconverting conformers. Slow exchange, on the TET ^{19}F-NMR chemical shift timescale, between the states I and A enabled a quantitative characterization of this rate process. Large values for ΔH_0 (Table 1) and an exchange rate slower than 10 S^{-1} (Figures 3–5) indicate that the interconversion entails major structural rearrangements, which likely involve polypeptide backbone segments.[11] Furthermore, the near-identical values of ΔH_0 for different ligands bound to the receptor (Table 1) indicate that the equilibrium between the two states is an intrinsic property of the receptor, so that binding of different orthosteric ligands, allosteric effectors, and possibly of cytoplasmic partner proteins would result in shifts of this pre-existing equilibrium. Comparison with recent related studies of β_2AR in DDM micelles shows that TET-labeling provides different information from NMR experiments using either a different ^{19}F-label, 3-bromo-1,1,1-trifluoroacetone (BTFA), on Cys 265[12] or ^{13}C-labeled Met 82,[13] which both provided evidence for two or multiple states of β_2AR in fast exchange on the respective chemical shift time scales. Results obtained by combining BTFA-labeling of Cys 265 with the use of the detergent maltose-neopentyl-glycol (MNG-3) were interpreted in terms of slow exchange between at least three states of β_2AR.[12] Different experimental approaches thus appear to provide complementary information on the β_2AR system, and one can look forward to continued studies of the dynamics of GPCRs with a variety of different reporter groups, including investigations of possible modulation of the protein conformational equilibria by allosteric effectors.

Experimental Section

The TET-labeled β_2AR constructs used in this study were expressed and purified as previously described.[4] Formoterol and norepinephrine were obtained commercially from Toronto Research Chemicals and Sigma, respectively. For the NMR experiments the β_2AR solutions were concentrated to 225 μl, using Vivaspin-2 concentrators (Sartorius), and 25 μl D_2O was added before transfer into Shigemi NMR tubes (Shigemi Inc., Allison Park, PA).

^{19}F NMR spectra were obtained with a Bruker AVANCE 600 spectrometer (Bruker, Billerica, MA), using a QCI ^{1}H/^{19}F–^{13}C/^{15}N quadruple resonance cryoprobe with shielded z-gradient coil. The sample temperature was measured with a standard calibration sample of 4% methanol in methanol-d_4. The ^{19}F-chemical shifts were calibrated using the internal standard TFA.

1D ^{19}F-NMR experiments were recorded with a data size of 1024 complex points, an acquisition time of 51 ms, and 24576 scans per experiment. 1D ^{19}F-NMR pre-saturation experiments were recorded with the same acquisition parameters, except that 49152 scans were collected. The duration of the cw pre-irradiation period and its field strength were 500 ms and 0.7 kHz, respectively. 2D [^{19}F,^{19}F]-EXSY experiments were recorded with a data size of 1024 and 32 complex points in the direct and indirect dimensions, respectively; 1204 scans were accumulated per increment.

Longitudinal spin relaxation times, T_1, were determined using the ^{19}F inversion recovery experiment[14] as implemented in the standard Bruker pulse program library (t1irpg, version 1.11). Six experiments with variable delays between 50 ms and 1s were recorded with a recovery delay of 2s and accumulation of 8192 scans per increment. All other parameters were the same as for the 1D ^{19}F-NMR experiments. The software xmgrace 5.1 (plasma-gate.weizmann.ac.il/Grace) was used for the data analysis. T_1 values were determined by fitting the peak volumes in the ^{19}F inversion–recovery experiment with the function $(1 - \exp(-T/T_1))$, where T is the variable delay in the t1irpg pulse sequence.

Major steps in the handling of the 1D and 2D ^{19}F-NMR datasets were to zero-fill the time domain data to twice the measured size, and to multiply the expanded free induction decays with an exponential function with a 30 Hz line-broadening factor.

To deconvolute overlapping signals (Figures 1 and 4), the ^{19}F-NMR spectra were fitted with a double-Lorentzian function, as implemented in the curve-fitting module of xmgrace 5.1. The quality of the fits was examined visually by estimating the residual difference between the experimental data and the result of the model calculation.

The pre-saturation data recorded with apo- β_2AR (C265A, ^{TET}C327, C341A) were analyzed based on model calculations with Equation (9), using the parameters given in the caption to Figure 5.

Acknowledgments

This work was supported by the NIH Roadmap initiative grant P50 GM073197 for technology development and the PSI:Biology grant U54 GM094618 for the GPCR-Network. KW is the Cecil H. and Ida M. Green Professor of Structural Biology at The Scripps Research Institute. We thank Katya Kadyshevskaya for help with the illustrations.

Appendix

The time-dependent Bloch equations for a two-site exchange process in the presence of a weak radio-frequency field with strength ω_1 and irradiation frequency ω_{rf}, as used in the data analysis of Figure 5, can be written in the form[10]

$$\frac{d\mathbf{m}}{dt}=\mathbf{b}+\mathbf{C}\cdot\mathbf{m}. \quad (5)$$

m and **b** are 6-dimensional vectors,

$$\mathbf{m}=\left(u^A, v^A, M_z^A, u^I, v^I, M_z^I\right)^{\mathrm{T}} \quad (6)$$

and

$$\mathbf{b}=\left(0, 0, \alpha_A M_0^A, 0, 0, \alpha_I M_0^I\right)^{\mathrm{T}}. \quad (7)$$

u^A and u^I are the magnetization components in-phase with the rotating field, v^A and v^I are the quadrature components, M_z^A and M_z^I are the longitudinal magnetizations, the coefficients α_A and α_I are the inverse of the longitudinal spin relaxation rates, $1/T_1^A$ and $1/T_1^I$, and M_0^A and M_0^I are the longitudinal magnetization values at t = 0. In the 6 × 6-dimensional matrix **C,**

$$\mathbf{C}=\begin{pmatrix} -\beta_A - k_1 & -\Delta\omega_A & 0 & k_{-1} & 0 & 0 \\ \Delta\omega_A & -\beta_A - k_1 & -\omega_1 & 0 & k_{-1} & 0 \\ 0 & \omega_1 & -\alpha_A - k_1 & 0 & 0 & k_{-1} \\ k_1 & 0 & 0 & -\beta_I - k_{-1} & -\Delta\omega_I & 0 \\ 0 & k_1 & 0 & \Delta\omega_I & -\beta_I - k_{-1} & -\omega_1 \\ 0 & 0 & k_1 & 0 & \omega_1 & -\alpha_I - k_1 \end{pmatrix}, \quad (8)$$

$\Delta\omega_A$ and $\Delta\omega_I$ are the offsets from the irradiation frequency, $\Delta\omega_A = \omega_A - \omega_{rf}$ and $\Delta\omega_I = \omega_I - \omega_{rf}$, β_A and β_I are the inverse of the longitudinal spin relaxation rates, $1/T_1^A$ and $1/T_1^I$, respectively, and k_1 and k_{-1} are the rate constants for forward and return exchange (Equation (2)).

A general solution of Equation (5) is given by

$$\mathbf{m}=-\mathbf{C}^{-1}\cdot\mathbf{b}+\exp\{\mathbf{C}\cdot\mathbf{t}\}(\mathbf{m_0}+\mathbf{C}^{-1}\cdot\mathbf{b}), \quad (9)$$

where $\mathbf{m}_0$ is the vector of initial values at t = 0. With the use of eigenvalues and eigenvectors the matrix exponential in Equation (9) takes the form

$$\exp\{\mathbf{C}\cdot t\}=\mathbf{X}\cdot diag(\mathbf{e}^{\lambda_1\mathbf{t}}, \ldots, \mathbf{e}^{\lambda_6\mathbf{t}})\cdot\mathbf{X}^{-1}. \quad (106)$$

X is the matrix containing the eigenvectors of **C**, and $diag(e^{\lambda_1 t}, \ldots, e^{\lambda_6 t})$ is a 6 × 6 dimensional diagonal matrix that contains the exponentials of the eigenvalues for **C**, *i.e.*, λ_1, …λ_6.

References

1. a) Cherezov V, Rosenbaum DM, Hanson MA, Rasmussen SG, Thian FS, Kobilka TS, Choi HJ, Kuhn P, Weis WI, Kobilka BK, Stevens RC. Science. 2007; 318:1258–1265. [PubMed: 17962520]

b) Rasmussen SG, DeVree BT, Zou Y, Kruse AC, Chung KY, Kobilka TS, Thian FS, Chae PS, Pardon E, Calinski D, Mathiesen JM, Shah ST, Lyons JA, Caffrey M, Gellman SH, Steyaert J, Skiniotis G, Weis WI, Sunahara RK, Kobilka BK. Nature. 2011; 477:549–555. [PubMed: 21772288] c) Jaakola VP, Griffith MT, Hanson MA, Cherezov V, Chien EY, Lane JR, Ijzerman AP, Stevens RC. Science. 2008; 322:1211–1217. [PubMed: 18832607] d) Xu F, Wu H, Katritch V, Han GW, Jacobson KA, Gao ZG, Cherezov V, Stevens RC. Science. 2011; 332:322–327. [PubMed: 21393508] e) Palczewski K, Kumasaka T, Hori T, Behnke CA, Motoshima H, Fox BA, Le Trong I, Teller DC, Okada T, Stenkamp RE, Yamamoto M, Miyano M. Science. 2000; 289:739–745. [PubMed: 10926528] f) Scheerer P, Park JH, Hildebrand PW, Kim YJ, Krauss N, Choe HW, Hofmann KP, Ernst OP. Nature. 2008; 455:497–502. [PubMed: 18818650]

2. a) Ghanouni P, Gryczynski Z, Steenhuis JJ, Lee TW, Farrens DL, Lakowicz JR, Kobilka BK. J Biol Chem. 2001; 276:24433–24436. [PubMed: 11320077] b) Ghanouni P, Steenhuis JJ, Farrens DL, Kobilka BK. Proc Natl Acad Sci U S A. 2001; 98:5997–6002. [PubMed: 11353823] c) Gether U, Ballesteros JA, Seifert R, Sanders-Bush E, Weinstein H, Kobilka BK. J Biol Chem. 1997; 272:2587–2590. [PubMed: 9006889] d) Swaminath G, Xiang Y, Lee TW, Steenhuis J, Parnot C, Kobilka BK. J Biol Chem. 2004; 279:686–691. [PubMed: 14559905] e) Yao XJ, Velez Ruiz G, Whorton MR, Rasmussen SG, DeVree BT, Deupi X, Sunahara RK, Kobilka B. Proc Natl Acad Sci U S A. 2009; 106:9501–9506. [PubMed: 19470481] f) Granier S, Kim S, Shafer AM, Ratnala VR, Fung JJ, Zare RN, Kobilka B. J Biol Chem. 2007; 282:13895–13905. [PubMed: 17347144] g) Yao X, Parnot C, Deupi X, Ratnala VR, Swaminath G, Farrens D, Kobilka B. Nat Chem Biol. 2006; 2:417–422. [PubMed: 16799554] h) Swaminath G, Deupi X, Lee TW, Zhu W, Thian FS, Kobilka TS, Kobilka B. J Biol Chem. 2005; 280:22165–22171. [PubMed: 15817484]
3. a) Klein-Seetharaman J, Getmanova EV, Loewen MC, Reeves PJ, Khorana HG. Proc Natl Acad Sci U S A. 1999; 96:13744–13749. [PubMed: 10570143] b) Loewen MC, Klein-Seetharaman J, Getmanova EV, Reeves PJ, Schwalbe H, Khorana HG. Proc Natl Acad Sci U S A. 2001; 98:4888–4892. [PubMed: 11320239]
4. Liu JJ, Horst R, Katritch V, Stevens RC, Wüthrich K. Science. 2012; 335:1106–1110. [PubMed: 22267580]
5. Atkins, PW. Physical chemistry. 5. Oxford University Press; Oxford, UK: 1995. p. 285
6. Dunitz JD. Chem Biol. 1995; 2:709–712. [PubMed: 9383477]
7. a) Jeener J, Meier BH, Bachmann P, Ernst RR. J Chem Phys. 1979; 71:4546–4553.b) Meier BH, Ernst RR. J Am Chem Soc. 1979; 101:6441–6442.c) Li H, Frieden C. Biochemistry. 2006; 45:6272–6278. [PubMed: 16700539]
8. Forsen S, Hoffman RA. J Chem Phys. 1963; 39:2892–2901.
9. Palmer AG 3rd, Kroenke CD, Loria JP. Methods Enzymol. 2001; 339:204–238. [PubMed: 11462813]
10. a) Bloch F. Phys Rev. 1946; 70:460–474.b) Bloch F, Hansen WW, Packard M. Phys Rev. 1946; 70:474–485.c) McConnell HM. J Chem Phys. 1958; 28:430–431.
11. Shaw DE, Maragakis P, Lindorff-Larsen K, Piana S, Dror RO, Eastwood MP, Bank JA, Jumper JM, Salmon JK, Shan Y, Wriggers W. Science. 2010; 330:341–346. [PubMed: 20947758]
12. a) Chung KY, Kim TH, Manglik A, Alvares R, Kobilka BK, Prosser RS. J Biol Chem. 2012; 287:36305–36311. [PubMed: 22893704] b) Kim TH, Chung KY, Manglik A, Hansen AL, Dror RO, Mildorf TJ, Shaw DE, Kobilka BK, Prosser RS. J Am Chem Soc. 201310.1021/ja404305k
13. a) Kofuku Y, Ueda T, Okude J, Shiraishi Y, Kondo K, Maeda M, Tsujishita H, Shimada I. Nat Commun. 2012; 3:1045. [PubMed: 22948827] b) Nygaard R, Zou Y, Dror RO, Mildorf TJ, Arlow DH, Manglik A, Pan AC, Liu CW, Fung JJ, Bokoch MP, Thian FS, Kobilka TS, Shaw DE, Mueller L, Prosser RS, Kobilka BK. Cell. 2013; 152:532–542. [PubMed: 23374348]
14. a) Luck LA, Vance JE, OConnell TM, London RE. J Biomol NMR. 1996; 7:261–272. [PubMed: 8765734] b) Canet D, Levy GC, Peat IR. J Magn Reson. 1975; 18:199–204.

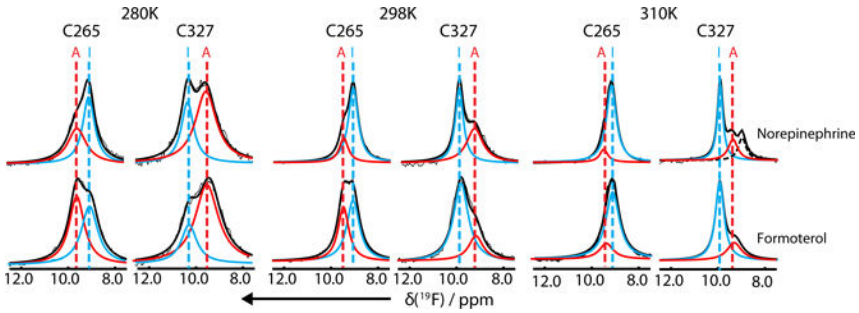

Figure 1.

1D ^{19}F-NMR spectra at 280 K, 298 K and 310 K of the complexes with the partial agonist norepinephrine (upper row) and the full agonist formoterol (lower row) of β_2AR(^{TET}C265, C327S, C341A) and β_2AR(C265A, ^{TET}C327, C341A) in mixed micelles of DDM and CHS 5:1. The ^{19}F-NMR assignments are indicated at the top. The experimental spectra were deconvoluted by non-linear least squares fits to a double-Lorentzian function. Thin and thick black lines show the experimental data and the fit function, respectively. The dotted black line in the spectrum of the norepinephine complex with β_2AR(C265A, ^{TET}C327, C341A) at 310 K represents the signal of micelle-bound free TET, which was subtracted from the experimental data before the non-linear least squares fit was obtained for this complex. $\nu(^{19}F)$ = 564.8 MHz, [β_2AR] = 25 μM, [DDM] = 7mM, [CHS] = 0.2 mM, pH = 7.5.

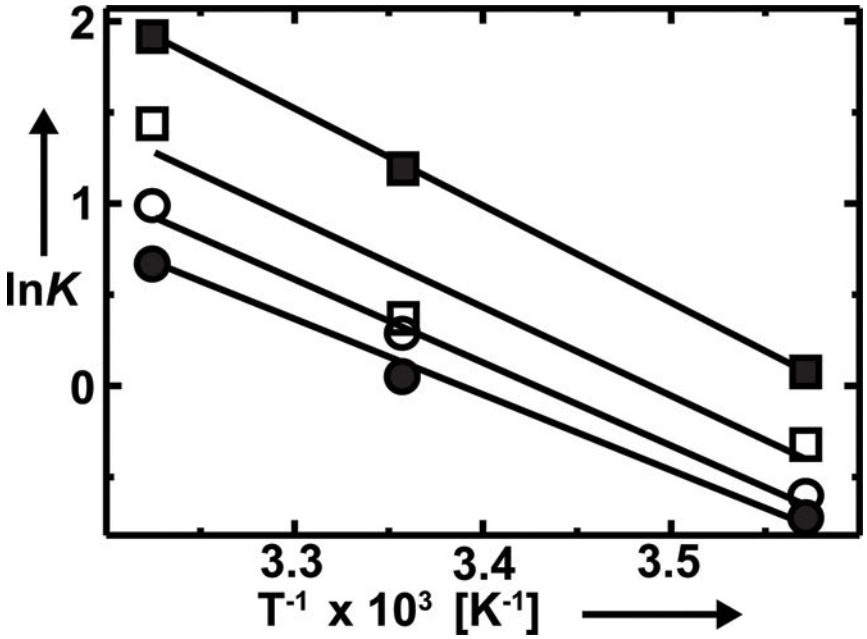

Figure 2.

van't Hoff plots for the interconversion between the active state (A) and the inactive state (I) of β_2AR(^{TET}C265, C327S, C341A) and β_2AR(C265A, ^{TET}C327, C341A) in the complexes with norepinephrine and formoterol. The apparent equilibrium constants, *K*, plotted along the vertical axis were obtained from the ratios of the peak volumes of the signals A and I in the ^{19}F-NMR spectra of Figure 1. (■) β_2AR(^{TET}C265, C327S, C341A) in complex with formoterol, (□) β_2AR(^{TET}C265, C327S, C341A) in complex with norepinephrine, (●) β_2AR(C265A, ^{TET}C327, C341A) in complex with formoterol, (○) β_2AR(C265A, ^{TET}C327, C341A) in complex with norepinephrine. The straight lines represent linear least squares fits of the experimental data, from which the molar enthalpy and entropy differences were obtained (Table 1).

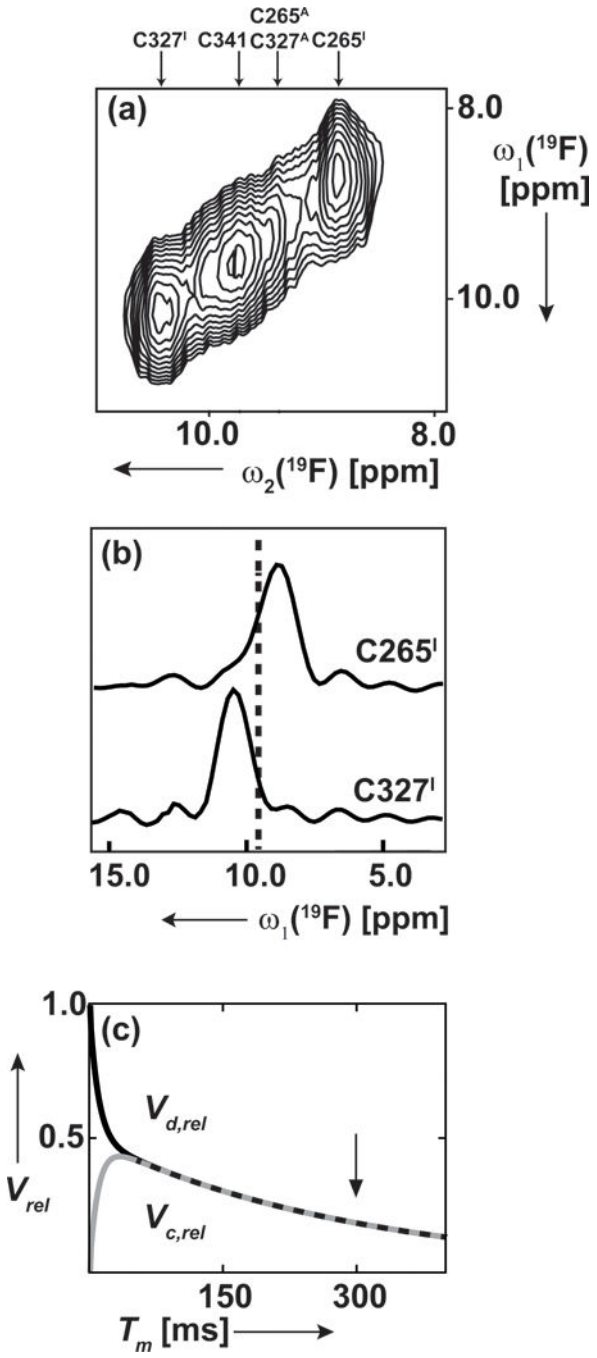

Figure 3.

2D [^{19}F,^{19}F]-EXSY experiments with the isoproterenol complex of wild type β_2AR (^{TET}C265, ^{TET}C327, ^{TET}C341) in mixed micelles of DDM and CHS 5:1. (a) Contour plot. At the top the chemical shifts of five previously assigned peaks[4] are indicated, i.e., the inactive state (I) and the activated state (A) of each of ^{TET}C265 and ^{TET}C327, and a single signal of ^{TET}C341. ν(^{19}F) = 564.8 MHz, [β_2AR] = 25 μM, [DDM] = 1 mM, [CHS] = 0.2 mM, pH = 7.5, T = 280 K. (b) 1D cross-sections taken at the chemical shift positions of C265^{I} and C327^{I}. A dotted vertical line indicates the position where cross-peaks C265^{I}–

C265^{A} and C327^{I}–C327^{A} would be expected (see text). (c) Model calculation of relative NMR peak volumes, V_{rel}, at variable EXSY mixing times, T_m. V_d and V_c are the volumes of corresponding diagonal peaks and exchange cross peaks, where $V_{d,rel} = V_d / V_o$, $V_{c,rel} = V_c / V_o$, and V_o is the diagonal peak volume at $T_m = 0$. The exchange rate, k_{ex}, was set to 10 s^{-1} and the longitudinal relaxation time, T_1, to 300 ms. The predicted values for the intensities of the diagonal peaks and the cross-peaks are shown by the black and grey lines, respectively. The arrow marks at the T_m-value of 300 ms, where the 2D [^{19}F,^{19}F]-EXSY spectrum shown in (a) and (b) was acquired.

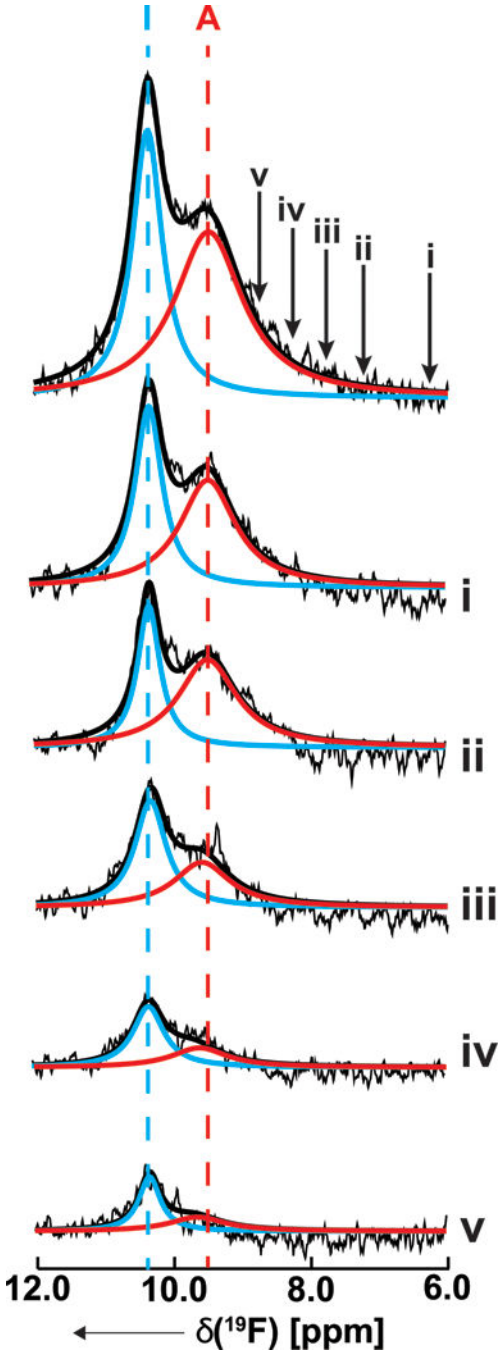

Figure 4.

1D ^{19}F-NMR saturation transfer experiments with apo-β_2AR(C265A, ^{TET}C327, C341A) in mixed micelles of DDM and CHS 5:1 used to measure the exchange rate between activated state (A) and inactive state (I) of β_2AR. Top trace: 1D ^{19}F-NMR spectrum, with peak volumes of the signals I at 10.3 ppm (cyan) and A at 9.5 ppm (red) obtained by deconvolution of the measured spectrum (thin black line showing noise) with non-linear least-squares fits of a double-Lorentzian function (thick black line). The arrows show the positions of the carrier frequency during cw pre-irradiation in the saturation transfer

experiments (i)–(v), where the duration and field strength for the cw irradiation were 500 ms and 0.7 kHz, respectively. $\nu(^{19}F)$ = 564.8 MHz, [β_2AR] = 25 μM, [DDM] = 1 mM, [CHS] = 0.2 mM, pH = 7.5, T = 280 K.

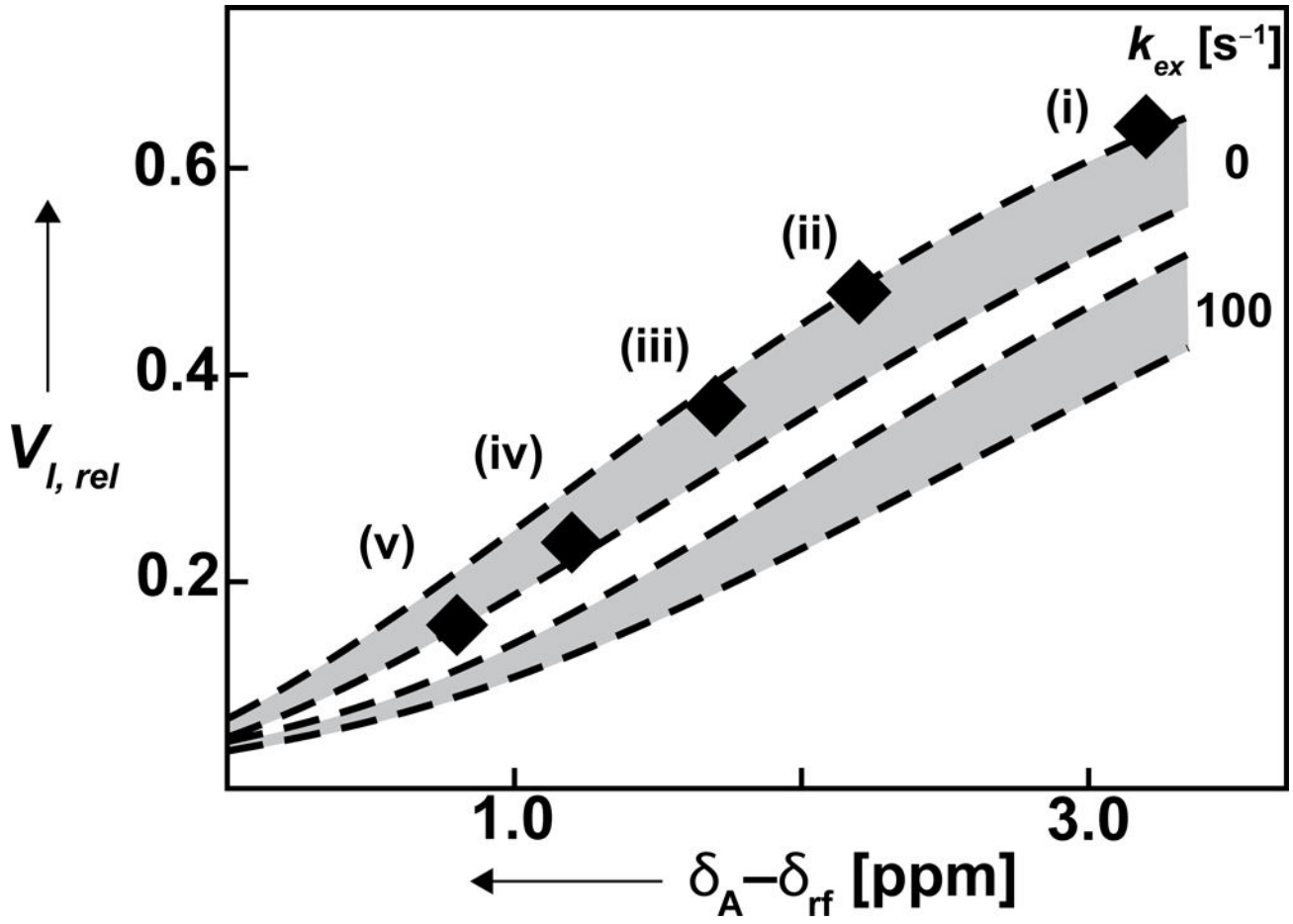

Figure 5.

Model simulations of the attenuation of the intensity of signal I in the NMR spectra of Figure 4 by off-resonance continuous wave (cw) pre-irradiation at the chemical shifts i to v. The relative peak volumes of the signal I in 1D ^{19}F-NMR saturation transfer experiments, $V_{I,rel} = V_I / V_{I,o}$, are plotted *versus* the frequency offset, $\delta_A - \delta_{rf}$. $V_{I,o}$ is the peak volume in the absence of pre-irradiation, and δ_A and δ_{rf} are the chemical shifts of the signal A and the carrier frequency for the cw pre-irradiation, respectively. The diamonds (i)–(v) represent the experimental data obtained from the corresponding spectra in Figure 4. The gray-shaded areas represent the results of model calculations of $V_{I,rel}$ values, using the formalism described in the Appendix. Simulations were performed for two values of the rate constant in Equation (2), i.e., $k_{ex} = 0$ s^{-1} and 100 s^{-1}, as indicated on the right, and the following parameters: Population of state A, $p_A = 0.45$; transverse relaxation times $T_2^A = 460 \pm 50$ ms and $T_2^I = 810 \pm 80$ ms; longitudinal relaxation times $T_1^A = 300 \pm 40$ ms and $T_1^I = 310 \pm 40$ ms. The width of the shaded areas represents the ranges of $V_{I,rel}$ -values that correspond to the uncertainty ranges of the T_1 and T_2 measurements (see text).

Table 1

Molar enthalpy differences, ΔH_0, and molar entropy differences, ΔS_0, for the interconversion between the activated and inactive states of the formoterol and norepinephrine complexes of β_2AR (^{TET}C265, C327S, C341A) and β_2AR(C265A, ^{TET}C327, C341A) solubilized in DDM/CHS mixed micelles at pH 7.5.

β_2AR complex	ΔH_0 [kJ/mol]	ΔS_0 [kJ/mol•K]
265/formoterol	40 ± 11	0.141 ± 0.40
265/norepinephrine	44 ± 1	0.159 ± 0.40
327/formoterol	38 ± 2	0.130 ± 0.10
327/norepinephrine	35 ± 3	0.117 ± 0.10